

# **Part One**

## **Fundamentals, Modeling, and Experimental Investigation of Photocatalytic Reactions for Direct Solar Hydrogen Generation**



# 1

## Solar Hydrogen Production by Photoelectrochemical Water Splitting: The Promise and Challenge

Eric L. Miller

*Hawaii Natural Energy Institute, University of Hawaii at Manoa, Honolulu, HI, USA,  
Email: ericm@hawaii.edu*

### 1.1 Introduction

Photoelectrochemical (PEC) water splitting, using sunlight to break apart water molecules into constituent hydrogen and oxygen gases, remains one of the “holy grail” technologies for clean and renewable hydrogen production. Hydrogen is an extremely valuable chemical commodity, not only in today’s industrial marketplace, but even more so in the emerging *green economies* so vital to the future of our planet and its people. “Green” futures will need to rely less and less on fossil fuels, and more and more on solar, wind, geothermal and other renewable energy resources. Hydrogen is envisioned as a primary media for the storage and distribution of energy derived from this renewable portfolio. To achieve the vision, much work is needed in the development of new, more practical technologies and infrastructures for hydrogen production, storage, delivery and utilization. Non-polluting technologies for large-scale hydrogen production utilizing renewable energy are of particular importance.

Among the viable renewable hydrogen-production approaches, PEC water splitting remains one of the most intriguing, yet one of the most elusive. A PEC system combines the harnessing of solar energy and the electrolysis of water into a single semiconductor-based device. Sunlight plus water gives us clean hydrogen plus oxygen. It sounds good, but it’s not all that easy. When a PEC semiconductor device is immersed in a water-based solution, solar energy can be

converted directly to electrochemical energy for splitting the water. This will only happen, however, if key criteria are all met. The semiconductor material must efficiently absorb sunlight and generate sufficient photovoltage to split water, while the semiconductor interface must be favorable to sustaining the hydrogen and oxygen gas evolution reactions. In addition, the PEC system needs to remain stable in solution, and must be cheap for any large-scale deployment.

This sounds like a very tall, complicated order, which in fact it is! No known semiconductor system achieves *all of the above criteria*, though some have come close. Multijunction PEC devices based on III–V semiconductor technology have been demonstrated at National Renewable Energy Laboratory (NREL) with impressive solar-to-hydrogen conversion efficiencies exceeding 16% [1]. Unfortunately, these devices lack long-term stability, and moreover III–V semiconductors are *very expensive* [2]! Lower-cost PEC devices based on thin-film semiconductors have been demonstrated, with stable hydrogen conversion efficiencies in the 3–5% range [3,4], but progress has plateaued at this efficiency level for quite some time. Important breakthroughs are needed in the development of new PEC materials and devices before practical PEC hydrogen production becomes a reality. Fortunately, the scientific community seems unable to resist the daunting challenge. Across the United States and around the world, the newest scientific techniques in materials theory, synthesis and characterization are being brought to the table, and powerful synergies among researchers in the PEC, photovoltaics and nanotechnology fields are emerging in collaborative pursuit of the needed breakthroughs.

Is this really a “holy grail?” PEC offers the potential for efficiently harnessing solar energy to produce high-purity hydrogen from water, at low operating temperatures, with no carbon emissions and using low-cost materials – definitely worth the quest! This chapter presents a brief overview of the PEC hydrogen-production research goals, progress and ongoing hurdles. A broad palette of topics, including hydrogen, solar-energy conversion, semiconductor materials and electrochemistry, are brought together to illustrate the promise and the challenge of PEC.

## 1.2 Hydrogen or Hype?

Hydrogen has become a hot topic in recent years, both in political and scientific circles. A national spotlight was cast on hydrogen in Former President George W. Bush’s State of the Union Speech in 2004, which featured such memorable quotes as: “America can lead the world in developing clean, hydrogen powered automobiles” and “With a new national commitment, our scientists and engineers will overcome obstacles to taking these cars from laboratory to showroom” [5]. From a completely different perspective, energy expert Joseph J. Romm in his book *The Hype About Hydrogen* asserts: “Neither government policy nor business investment should be based on the belief that hydrogen cars will have meaningful commercial success in the near- or medium-term” [6].

Whatever spin you take on the future importance of hydrogen, the world’s most abundant element is in fact an extremely valuable chemical commodity today. In the contemporary industrial marketplace, hydrogen is a high-volume chemical with US production exceeding 5 000 000 kg annually. Important industry uses include the production of chemicals, processing of materials, semiconductor manufacturing, generator cooling and fertilizer production, among others. Hydrogen’s low density, high thermal conductivity and strong chemical reducing properties make it ideal for such applications. To satisfy the industrial demand,

current hydrogen production relies primarily on fossil-fuel technologies. Worldwide, over 95% of hydrogen is produced from natural gas, oil or coal. US production relies mainly on steam–methane reforming.

Of course, fossil fuels are vulnerable to dwindling availability and rising cost, and result in carbon emissions and other forms of environmental contamination. All current industries, including those utilizing hydrogen, suffer the risks and disadvantages of our current *fossil-fuel economy*. In any event, new, cleaner and long-term approaches to hydrogen production will need to be considered. The motivation increases exponentially if *hydrogen economy* proponents have their way [7–10]!

In a future hydrogen economy, hydrogen is envisioned as the ideal energy-carrier for the storage and distribution of renewable energy resources such as solar, wind, geothermal, hydroelectric and others. Using fuel-cell or combustion-engine technologies, hydrogen can be converted simply and cleanly to power or heat with no carbon emissions, and with water as the primary by-product. As an added bonus, hydrogen is nature’s most abundant element. Unfortunately, it exists primarily in strongly bonded chemical compounds, and extracting it is a difficult and energy-intensive process. With current technologies, it would be difficult to economically produce, store or utilize this ideal energy carrier. An enormous amount of technology and infrastructure development would be needed to attain a pure hydrogen economy.

Realistically, a green economy will emerge comprising a broad portfolio of alternative energy sources and carriers, including hydrogen. As our present reliance on petroleum-based fossil fuels become increasingly difficult to sustain, both economically and environmentally, this will become inevitable. As a result, new, more distributed approaches to national and world energy management will take hold. Different locations rich in their own renewable resources can manufacture energy currencies such as electricity or hydrogen for large-scale distribution to the broader energy marketplace. Electricity is a key energy carrier today, and will remain so long into the future. Hydrogen, however, will also emerge in an important complementary role, providing important benefits in large-scale energy storage and long-distance distribution.

Bottom line, without hype: hydrogen is valuable today, and will become increasingly valuable as an energy carrier with the future development of new renewable-energy production and distribution infrastructures. In the process, new and improved technologies will emerge for the economical and environmentally friendly production, storage, delivery and utilization of hydrogen. Production technologies using solar energy to split water are enormously attractive, motivating, for example, accelerated PEC research and development.

## 1.3 Solar Pathways to Hydrogen

### 1.3.1 The Solar Resource

In discussing the world energy situation of the early twentieth century, Thomas Edison once said: “I’d put my *money* on the sun and solar energy. What a source of power! I hope we don’t have to wait ’til oil and coal run out before we tackle that” [11]. It’s almost 100 years later, and we are still hoping, perhaps now with a little more urgency. The sun is, in fact, the ultimate renewable energy resource, continuously bombarding earth with about 180 000 000 000 000 000 W (or 180 000 TW) of radiant power, enough to power 3 quadrillion 60 W light bulbs [12,13]! About 50 000 TW of this is directly reflected back to space, and 82 000 TW is absorbed by earth

and re-emitted as heat. Of this, 36 000 TW is absorbed at the earth's land masses, where terrestrial-based solar-energy conversion plants could be installed practically.

To put this in perspective, our society on average consumes 13–15 TW, with some predictions doubling this consumption rate by the year 2060 [14]. Although these numbers are staggering, they still represent a small fraction of the sun's influx of radiant power. It might seem that solar energy alone could satisfy our insatiable hunger for energy. Of course, it is not that simple. The planet relies on the sun for many things, including sustaining plant-life and driving its weather patterns, and our voracious energy demands are relatively low on nature's priority list. Still, despite the abundance of spare solar energy at our disposal, large-scale conversion is currently quite costly and somewhat problematic. At peak times of daylight, the solar intensity available for terrestrial conversion scales to approximately  $1000 \text{ W m}^{-2}$ . Large collection areas and significant landmass would therefore be needed for commercial-scale power production. Such expansive commercial deployment requires an enormous capital investment. For example, commercial photovoltaic technologies today can convert sunlight to electricity at efficiencies between 10 and 20%, at \$2–5 per installed watt [15]; a single Gigawatt plant would cost billions of dollars and span over 2500 acres! Even worse, this gargantuan installation would be a sleeping giant at night and under severe cloud cover.

There are certainly practical difficulties and challenges, yet our sun is still the most generous renewable resource, and the most underutilized in modern society. Currently, less than 0.05% of the world energy production is from solar-energy plants, though this number is on the rise of late [16]. Encouragingly, improved technologies for solar-energy conversion, storage and utilization are emerging to make their impact on the world energy scene. New and improved solar-to-electric and solar-to-hydrogen conversion technologies are all poised to be part of the new energy mix.

### 1.3.2 Converting Sunlight

In converting sunlight, whether to electricity or to hydrogen, fundamental thermodynamic principles govern the energy-conversion process. As illustrated in Figure 1.1, the sun can be viewed as a black body radiating at a temperature of 5780 K, while the earth, as a *black body*, radiates at 300 K. The Carnot limit between these source and sink temperatures is readily calculated to 95%, representing the amount of radiant energy that can be converted into other more useable energy forms. This is very encouraging! A lot of solar energy available, and in theory most of it can be converted for practical end-uses. Unfortunately, however, actually converting sunlight is always further limited by unavoidable losses associated with available energy-conversion routes. Thermodynamically, efficiency is lost with every added conversion step in the process.

The sun transmits energy radiatively via photons, quantum particles of light with discrete energy content. Figure 1.2 shows the standard AM1.5<sub>global</sub> atmosphere-filtered solar spectrum [17] indicating the range of photon energies comprising sunlight, and the distribution of energy transmitted by these photons. The solar photons ( $\gamma$ ) reaching earth readily interact with electrons, energizing them to excited states ( $e^-$ ), as illustrated in Figure 1.1. Two basic routes for energy conversion of the photoexcited electrons are also depicted. In the *solar-thermal route*, the energized electrons thermalize to their surroundings, converting the energy to heat ( $v$ ). This thermal energy can be converted further, for example, using heat-engines to produce work, though now restricted by a lower Carnot limit based on an intermediate source temperature.

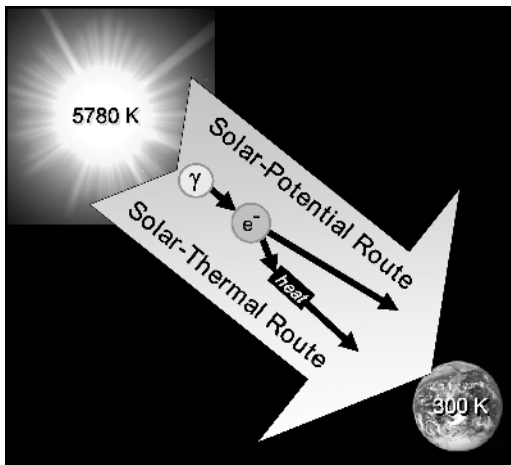


**Figure 1.1** Black-body representation of the sun and earth showing solar-energy conversion routes.

Alternatively, in the *solar-potential route*, the elevated electrochemical potential of the energized electrons can directly drive further conversion processes, for example, producing electricity or chemical products. Thermal energy is not being converted, so no additional Carnot limits are imposed.

### 1.3.3 Solar-Thermal Conversion

In solar-thermal conversion systems, concentrated sunlight produces high temperatures to drive heat-engines for generating mechanical work, electrical energy, or chemical products.

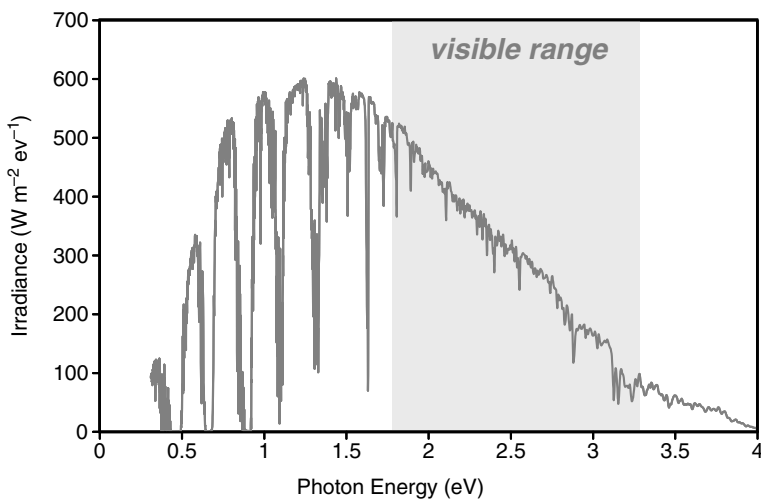


**Figure 1.2** The AM1.5<sub>global</sub> spectrum shown as a function of photon energy. The range of photons in visible light is highlighted.

A good example of this route is the solar-thermal production of electricity. Concentrating solar thermal (CST) systems employ mirrored troughs, dishes or heliostats for focusing sunlight to heat working fluids of a gas- or liquid-phase turbine cycle. Solar concentration up to  $1000\times$  and working-fluid temperatures in the  $250\text{--}1100\text{ }^\circ\text{C}$  range are common. Conversion efficiencies, governed by the Carnot limit, can be quite high for the highest operational temperatures, but significant materials issues arise. Exotic refractory materials are needed, adding significant cost to plant production, operations and maintenance. One important advantage of solar-thermal production of electricity is that conventional generators and infrastructure can be used, facilitating plant design and implementation. Thermal storage of the energy via storage of the heated fluid can also be an advantage, especially in the higher-temperature systems. Recently, an experimental CST 25 kW system installed at Sandia National Laboratories has reported solar-to-electric efficiencies as high as 31% [18]. Larger-scale installations, such as the 50 MW Andasol plant in Spain operate at gross efficiencies closer to 3% [19].

Another example of solar-thermal energy conversion is the production of hydrogen as a chemical by-product of solar-thermochemical cycles (STC). Concentrated sunlight provides the net heat for driving a multistep thermochemical process involving the splitting of water into hydrogen and oxygen gases. Many STC chemical cycles are known, including the sulfur-iodine [20,21] and copper-chlorine [22] cycles with reaction temperatures ranging up to 1200 K. High solar-to-hydrogen conversion efficiencies are possible, reported between 42–57% in the sulfur-iodine cycles, with a high-temperature step at 1123 K. The high-temperature, corrosive operating environment of all STC reactors, however, can be problematic, requiring specialized, and usually expensive materials, components and maintenance.

#### *1.3.4 Solar-Potential Conversion*

In the solar-potential route, photons in the incident solar light energize electrons, which can be converted directly to electrical or electrochemical energy. The primary example of the solar-potential conversion process is the photovoltaic (PV) production of electricity. Photons are absorbed in semiconductor materials where they excite electrons from the valence into the conduction band. These excited electrons, at elevated electrochemical potentials, can be extracted into an external circuit, directly converting the photon energy into electric energy. Though direct, the conversion is not without loss. Some of the excited electrons thermalize to their surroundings, causing waste heat. In efficient PV cells, however, this waste is minimal, resulting in moderate temperature rises. Operating temperatures in PV installations without concentration can be quite low, typically ranging from  $30\text{ to }80\text{ }^\circ\text{C}$ . This is a particularly attractive feature, since low-temperature plants do not require specialized materials, and are easy to operate and maintain. Another attractive feature of PV-generated electricity is the absence of mechanical “moving parts” common to the turbine systems in CST generation. Large-scale power electronics such as power inverters are needed, but these systems have become more efficient and robust in recent years. On the down side, PV semiconductor materials and systems are still relatively expensive. Although cumulative global installations of PV generation has reached over 1500 MW [15], the per-installed-watt price still exceeding \$3 is somewhat prohibitive in many economic sectors.

Other examples of solar-potential conversion include photoelectrochemical processes such as waste-water remediation, and the industrial synthesis of chemicals and synthetic fuels.

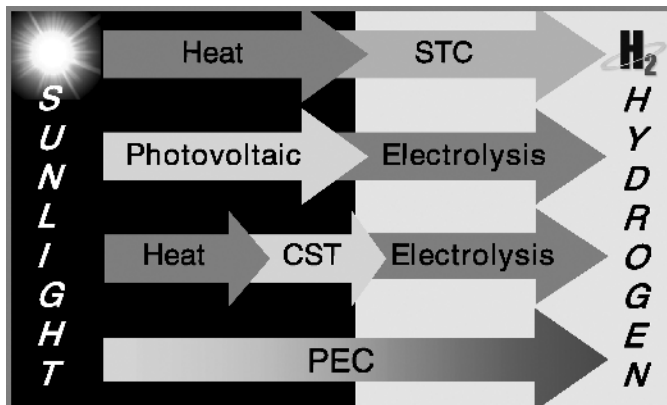


**Figure 1.3** Solar-to-hydrogen conversion pathways. (STC stands for solar-thermochemical, CST for concentrating solar-thermal, and PEC for photoelectrochemical).

Hydrogen production by PEC water splitting, an attractive low-temperature alternative to solar-to-hydrogen water splitting, falls into this category.

### 1.3.5 Pathways to Hydrogen

Using sunlight to split water for hydrogen production can follow several different conversion routes, as shown in Figure 1.3. The solar-thermal route is essentially a two-step process, with a photon-to-thermal energy-conversion step followed by a thermal-to-chemical conversion step. The other two-step process shown in the figure represents PV-electrolysis, where a photon-to-electric conversion step is followed by an electric-to-chemical conversion process. The three-step process represents a CST-electrolysis route, involving photon-to-heat, heat-to-electricity and electricity-to-chemical conversion steps. The final pathway depicted, representing a single-step direct conversion from photon-to-chemical energy, is the PEC water-splitting process. Other solar-to-hydrogen pathways are possible, including photobiological routes [23,24] and the ultra-high-temperature thermolysis route [25]. All pathways can contribute to renewable hydrogen production for future “green economies,” but economics will determine which will predominate.

From an economic viewpoint, it is important to remember that both hydrogen and electricity will be valuable as renewable-energy carriers in the future. Processes capable of producing both, such as PV-electrolysis and CST-electrolysis, could be advantageous. In fact, PV- and CST-electrolysis systems can be assembled today using off-the-shelf components. The electricity and the hydrogen produced would not be inexpensive, but this will change with further maturing of the technologies. It will remain vital to keep an eye on the alternative, even less-mature approaches. The solar-electrolysis routes comprise multiple conversion steps, with efficiency loss at each step. In terms of hydrogen production, the most direct conversion processes, such as PEC water splitting, could have some inherent performance advantages. PEC hydrogen production as a low-temperature single-stage process remains one of the front-running alternatives.

## 1.4 Photoelectrochemical Water-Splitting

### 1.4.1 Photoelectrochemistry

Photoelectrochemistry is a complex, and extremely rich scientific field drawing together fundamental concepts from chemistry, physics, optics, electronics and thermodynamics. In contrast with standard chemical processes involving interactions between chemical and ionic species, electrochemical processes can also involve interfacial interactions between ionic conductors, such as electrolyte solutions, and solid-state electronic conductors, such as semiconductors. Photoelectrochemical (PEC) processes comprise electrochemical systems exposed to light, where optical photons interact with the electrochemical reactions. In semiconductor photoelectrochemistry, photons typically create electron–hole pairs within the semiconductor that can react with redox chemistry at semiconductor/electrolyte interfaces. Although a complicated set of fundamental electrochemical and solid-state optoelectronic principles govern the behavior of such systems, some useful simplifications can be helpful in providing a broad overview of the PEC water-splitting process.

### 1.4.2 PEC Water-Splitting Reactions

Most texts on PEC water splitting will start with the simple two-electrode setup shown in Figure 1.4. In this canonical model, a light-sensitive semiconductor photoelectrode is immersed in an aqueous solution, with electrical wiring connected to a metallic counter-electrode. With exposure to sunlight, photogenerated electron–hole pairs in the semiconductor interact electrochemically with ionic species in solution at the solid/liquid interfaces. Photoexcited holes drive the oxygen-evolution reaction (OER) at the anode surface, while photoexcited electrons drive the hydrogen-evolution reaction (HER) at the cathode surface. Figure 1.4 depicts a *photoanode* system where holes are injected into solution at the semiconductor surface for evolving oxygen, while photoexcited electrons are shuttled to the counter-electrode where hydrogen is evolved. Conversely, in *photocathode* systems, electrons are injected into solution and hydrogen is evolved at the semiconductor surface, while oxygen is evolved at the counter-electrode. Similar to solid-state pn-junction solar cells, PEC photoelectrodes typically act as *minority carrier* devices [26,27]. The semiconductor/liquid junction, like the pn junction, allows the flow of minority carriers, while blocking majority-carrier flow. For this reason,

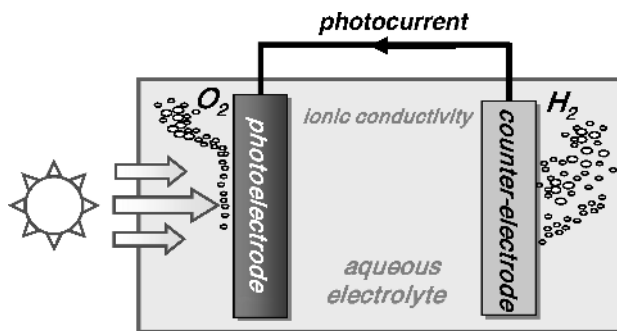
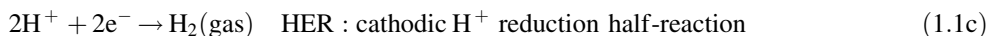
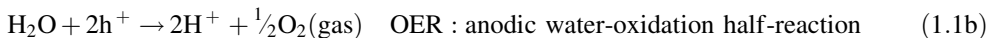
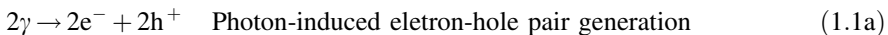


**Figure 1.4** Standard two-electrode setup for PEC water splitting, shown in the photoanode configuration with a separated counter-electrode.

n-type semiconductors allowing minority-carrier hole injection are better suited as photoanodes, while p-type semiconductors are used as photocathodes.

In the PEC water-splitting process, oxygen evolution at the anode and hydrogen evolution at the cathode can be modeled as two electrochemical “half-reactions.” Both must be sustained simultaneously, coupled by their exchange of electrons in the solid state, and ions in solution. A simplified equation set describing the half-reactions in addition to the net conversion process can be written:



$$\Delta G^\circ = +237.18 \text{ kJ mol}^{-1} \quad \text{Standard Gibbs free energy} \quad (1.1e)$$

$$V_{\text{rev}}^\circ = \Delta G^\circ / nF = 1.23 \text{ V} \quad \text{Standard reversible potential} \quad (1.1f)$$

$$V_{\text{op}} = V_{\text{rev}}^\circ + \eta_a + \eta_c + \eta_\Omega + \eta_{\text{sys}} \quad \text{Operating voltage with overpotential losses} \quad (1.1g)$$

where  $\gamma$  is photon energy,  $e^-$  is an electron,  $h^+$  is a hole,  $\Delta G^\circ$  is the standard Gibbs free energy,  $V_{\text{rev}}^\circ$  is the standard reversible potential,  $n$  ( $=2$ ) is the number of electrons exchanged,  $F$  is the Faraday constant,  $V_{\text{op}}$  is the operational voltage,  $\eta_a$ ,  $\eta_c$ ,  $\eta_\Omega$ , and  $\eta_{\text{sys}}$ , are overpotentials associated with anode, cathode, ionic-conductivity and system losses, respectively.

Implicit in Equation Set 1.1, solid-state electrons/holes are exchanged between the anode and cathode through a conductive pathway (such as a wire), while  $\text{H}^+$  ion migration from anode to cathode is through the aqueous media. It is clear from the equation set that PEC water splitting is a delicate balancing act, where photon-energized electron–hole pairs under the right conditions can simultaneously drive the electrochemical half-reactions. In steady-state, the reactions in Equations 1.1b and 1.1c, must be sustained at the same reaction rate. Since  $\text{H}^+$  ions are generated at the anode surface and consumed at the cathode surface, unless these events are proceeding concurrently at identical rates, charge build-up will impede or even stop the entire process. A similar situation exists with the charge carriers in the solid state. The anodic half-reaction consumes two holes (i.e., supplies two electrons) while the cathode half-reaction consumes two electrons. These electrons must be shuttled from anode to the cathode via electrical current (e.g., through the interconnecting wire shown in Figure 1.4), and steady state cannot be maintained if anode and cathode reaction rates are not the same.

There are several additional key points that should be emphasized regarding the thermodynamic parameters included in Equation Set 1.1:

- $\Delta G^\circ = +237.18 \text{ kJ mol}^{-1}$  is the standard Gibbs free energy change, representing a thermodynamic minimum for splitting water into the constituent gases at standard conditions of  $25^\circ\text{C}$  and 1 bar. Since  $\Delta G^\circ$  is positive, energy needs to be supplied to the drive electrolysis process.

- $V_{\text{rev}}^{\circ} = 1.23 \text{ eV}$  is the corresponding reversible potential, indicating the minimum electrical potential needed to sustain reversible photoelectrolysis.
- Water splitting will *not* occur at a bulk potential of 1.23 V. This value does not take into account unavoidable process losses, including overpotential loss at the anode ( $\eta_a$ ), overpotential loss at the cathode ( $\eta_c$ ) or ionic conductivity losses in solution ( $\eta_{\Omega}$ ), in addition to other balance-of-system losses ( $\eta_{\text{sys}}$ ).
- The half-reactions described in Equations 1.1b and 1.1c are simplifications of more complex multistep electrochemical reaction pathways [28,29]. The electrode overpotential losses of these multistage reactions, including the effects of activation energy, kinetics and mass-transport can be substantial, commonly several tenths of volts. The water-oxidation reaction at the anode is the more complex and less facile reaction, so the anodic overpotential losses are more severe.
- Overpotential losses due to ionic conductivity in the solution can also be severe. These losses depend on solution properties, as well as electrode geometry and spacing. The splitting of *pure water* is particularly difficult, since the ionic conductivity, typically less than  $0.05 \text{ S m}^{-1}$ , is prohibitively low. Weak acid or alkaline solutions with conductivities exceeding  $10 \text{ S m}^{-1}$  are typically used to compensate, although this creates a more corrosive environment for the electrodes.
- $V_{\text{op}}$ , the operating voltage for water splitting, must exceed  $V_{\text{rev}}^{\circ}$  to compensate for all the losses, as indicated in Equation 1.1g. In practice, water electrolysis systems typically require operating voltages of 1.6–1.9 V, depending on gas-production rates [30,31].

The focus of Equation Set 1.1 is on electrochemical behavior and the losses in solution. Losses in the solid-state electrodes, including electron–hole-pair recombination losses and electronic conductivity losses, among others, also degrade system performance. To drive the water-splitting process, including all solution and electrode losses, the absorbed photons must induce sufficient electrochemical potential to the electron–hole pairs. The photoelectrolysis *balancing act* can be set into motion *only* if the photopotential requirement is met. Once in operation, the hydrogen evolution will be proportional to electron consumption, as per Equation 1.1c.

During steady-state operations, the solid-state shuttling of charges between anode and cathode represents a photon-induced current, or photocurrent, that is integrally tied to the hydrogen-producing performance of the PEC system. Explicitly from Equation 1.1c, two electrons are consumed in the evolution of one  $\text{H}_2$  molecule. The rate of hydrogen production is therefore half the rate of electron flow, in other words, half the photocurrent. This is technically written:

$$R_{\text{H}_2} = \frac{I_{\text{ph}}}{2e} = \frac{(J_{\text{ph}} \times \text{Area})}{2e} \Rightarrow J_{\text{ph}} = \left( \frac{R_{\text{H}_2}}{\text{Area}} \right) \times 2e \quad (1.2)$$

where  $R_{\text{H}_2}$  is the hydrogen production rate ( $\text{s}^{-1}$ ),  $I_{\text{ph}}$  is the photocurrent (A),  $e$  is the electronic charge (C), Area is the illuminated photoelectrode area,  $J_{\text{ph}}$  is photocurrent density ( $\text{A m}^{-2}$ ).

In Equation 1.2, the photocurrent density  $J_{\text{ph}}$  is normalized to the illuminated area of the photoelectrode, and is therefore inversely proportional to the incident photon flux. Upon closer look,  $J_{\text{ph}}$  is proportional to the ratio between the hydrogen production rate and the solar energy input. As a result, this parameter becomes particularly important when evaluating the solar-to-hydrogen conversion performance of a PEC system.

### 1.4.3 Solar-to-Hydrogen Conversion Efficiency

The chemical solar-to-hydrogen (STH) conversion efficiency of any solar-based hydrogen production system is defined as the ratio of the useable chemical energy in the generated hydrogen gas to the total solar energy delivered to the system. For steady-state operations, this is equivalent to the ratio of the *power output* to the *power input*. In words, this can be expressed:

$$\frac{P_{\text{out}}}{P_{\text{in}}} = \frac{(\text{hydrogen production rate}) \times (\text{hydrogen energy density})}{\text{solar flux integrated over illuminated area}} \quad (1.3)$$

Using the hydrogen-production rate from Equation 1.2, the Gibbs energy as the useful energy density of the hydrogen and an integrated solar flux of  $1000 \text{ W m}^{-2}$  for AM1.5<sub>global</sub> solar irradiation, the STH efficiency for a PEC system can be expressed:

$$\text{STH}(\%) = \frac{\Delta G R_{\text{H}_2}}{P_{\text{solar}} \times \text{Area}} = \frac{\Delta G \left( \frac{J_{\text{ph}} \times \text{Area}}{2e} \right)}{P_{\text{solar}} \times \text{Area}} \approx \underbrace{0.123 \times J_{\text{ph}} (\text{Am}^{-2})}_{\text{for AM1.5}_g \text{ solar irradiation}} = 1.23 \times J_{\text{ph}} (\text{mA cm}^{-2}) \quad (1.4)$$

The first ratio in Equation 1.4 is generic for any solar-to-hydrogen production system, while the second is derived specifically for PEC hydrogen processes. The third term, explicitly relating conversion efficiency to the photocurrent density, is calculated for a PEC system under AM1.5<sub>global</sub> solar illumination. In Equation 1.4, the use of the Gibbs free energy reflects chemical energy in the hydrogen that can be retrieved using an ideal fuel cell. This, in effect, calculates the lower-heating value (LHV), which is standard in practical comparisons between different fuels.

On the subject of standard efficiency terminology, numerous types of efficiency have been defined and employed throughout PEC literature [32–35], but extreme care needs to be taken in the appropriate application and interpretation of each. For valid side-by-side comparisons with other solar-to-hydrogen conversion technologies, the STH definitions in Equation 1.4 must be used. To be strictly correct, the hydrogen gas evolved should be collected and certified in any efficiency determination, since parasitic effects cannot be quantified in volume or photocurrent measurements alone. Alternative efficiency definitions have included three-terminal efficiencies, efficiencies specific to a limited range of photon wavelengths, and energy-saving efficiencies for externally biased systems. These can be extremely useful in characterization of PEC materials and interfaces, but cannot be equated with a system STH efficiency. STH calculations using the higher heating value (HHV) for hydrogen have been reported, founded on novel utilization schemes recovering the water's heat of condensation. These, however, do not conform to industry-standard reporting practices based on the LHV.

Independent of the heating value used, it is clear from Equation 1.4 that the PEC STH efficiency is *all about the photocurrent*. In contrast to solid-state solar cells, operated at the maximum power point (i.e., maximum product of photocurrent and photovoltage) for the best solar-to-electric conversion efficiency [36], the PEC cell should be operated at maximum photocurrent for best hydrogen-production performance. This becomes extremely important in the design and optimization of PEC semiconductor materials and devices. It is the *saturated photocurrent density* limit of a semiconductor that ultimately constrains the hydrogen production rate. For peak efficiency, sufficient photopotential must be generated in the device to drive the photocurrent into saturation. With all the built-in losses, this can be a difficult challenge.

### 1.4.4 Fundamental Process Steps

Losses affecting STH conversion efficiency are inherent in all processes occurring in the solid state, in solution and, often most importantly, at the interface. To help keep track of the loss mechanisms, it is useful to break down the PEC water-splitting dynamics into fundamental process steps, tracking events all along the way from the photon collection in the photoelectrode to the hydrogen release in solution. These basic steps can be summarized as follows:

1. **Photon Absorption/Charge Generation (solid-state):** Solar photons are absorbed in the semiconductor, creating excited charge carriers in the form of electron–hole pairs. Absorption losses are related to semiconductor bulk properties.
2. **Charge Separation and Transport (solid-state/interface):** Photoexcited electron–hole pairs must be separated spatially, and before recombining to lower energy states, must be transported to opposite contact surfaces for extraction. The separation mechanisms are tied to charge distributions in the solid state and at the interface. Transport losses are related to semiconductor defects and other mobility-limiting effects.
3. **Charge Extraction/Electrochemical Product Formation (interface):** Charge carriers transported to anode/cathode surfaces can be extracted into the water-oxidation/hydrogen-reduction half-reactions, respectively. Oxygen/hydrogen gas is produced, while hydrogen ions are consumed/formed. Interface losses are many, including poorly aligned energetics, reaction overpotentials and slow reaction kinetics.
4. **Electrochemical Product Management (solution):** Hydrogen and oxygen gas need to be removed from solution, while the hydrogen ion concentrations need to redistribute. Ionic conductivity losses as well as “bubble” losses (e.g., related to disruption of mass transport in solution and to possible light blockage) are present.

In a semiconductor photoelectrode system, photons are absorbed in the semiconductor bulk, and the photogenerated charge carriers (in the form of electron–hole pairs) are separated, transported and extracted due to the rectifying nature of the semiconductor/electrolyte junction. Not surprisingly, hydrogen production performance is strongly influenced both by semiconductor material properties and by junction characteristics.

## 1.5 The Semiconductor/Electrolyte Interface

### 1.5.1 Rectifying Junctions

In semiconductor-based PEC water-splitting systems, the semiconductor/electrolyte interface can form a *rectifying* junction, similar to the solid-state pn junctions or Schottky diode junctions used in solar cells. Such rectifying junctions exhibit built-in electric fields capable of separating excited charge carriers (i.e., electron–hole pairs) created by absorbed solar photons. In solid-state solar cells, this charge-separation mechanism drives photocurrents to produce electricity, while in the PEC case, the charge separation can drive the HER and OER half-reactions for water-splitting. In both cases, illumination creates extra photoexcited electron–hole pairs, which need to be separated and extracted before they recombine. Extraction of the photogenerated charge carriers with elevated electrochemical potentials in effect converts the solar energy to electricity or hydrogen. Many good sources of information

are available, detailing semiconductor material properties, solid-state junctions and solar cells [13,26,27,37–39], and these provide an excellent background for understanding fundamentals of rectifying junction formation and behavior.

### 1.5.2 A Solid-State Analogy: The $np^+$ Junction

Before tackling the semiconductor/electrolyte junction, it is interesting to consider the analogous solid-state  $np^+$  junction represented in Figure 1.5. In this device, the  $n$ -region is doped with *donor* atoms to provide an excess of free electrons, and the  $p^+$ -region is more heavily doped with *acceptor* atoms for a high concentration of holes. Carrier densities at equilibrium typically would be, for example,  $10^{15} \text{ cm}^{-3}$  for the  $n$ -region and  $10^{16} \text{ cm}^{-3}$  for the  $p^+$ -region. Figure 1.5 includes the classic band-diagram representation of the  $np^+$  device, with Figure 1.5a showing the separated semiconductors in thermal equilibrium. Consistent with the relative level of doping, Fermi levels ( $F$ ) are close to the conduction band (CB) in the  $n$ -region, and very close to valence band (VB) on the  $p^+$  side.

Figure 1.5b depicts the  $np^+$  junction formation as the two doped materials are brought together. At equilibrium, the Fermi levels align across the device, resulting in the band-bending

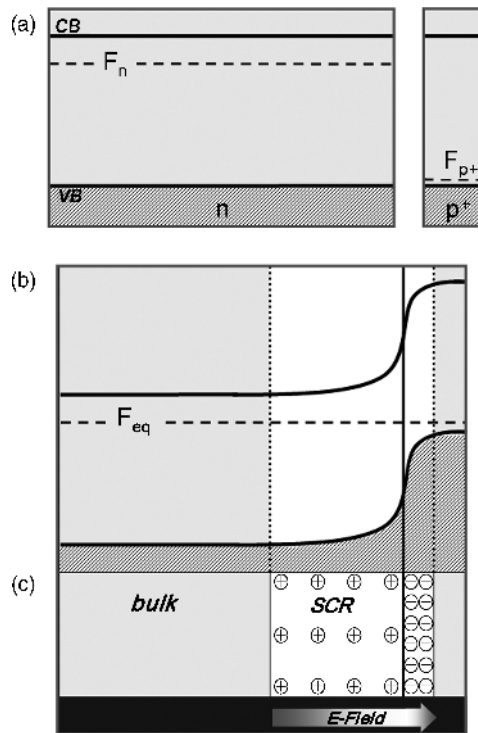


**Figure 1.5** Formation of the  $np^+$  solid-state rectifying junction showing: (a) materials before contact; (b) band diagram of junction formation and equilibration and (c) charge distributions and built-in electric field. ( $F_n$ ,  $F_{p^+}$  and  $F_{eq}$  represent Fermi levels in the isolated  $n$  and  $p^+$  regions, and in equilibrium after contact, respectively).

observed in the figure. Near the junction, free electrons from the n-side diffuse into the  $p^+$ -side, leaving behind the fixed positive charges of ionized donor atoms. Conversely, holes from the  $p^+$ -side diffuse into the n-region, exposing fixed negatively charged acceptor atoms. A *depletion region*, also known as a *space-charge region* (SCR), forms where free carrier diffusion is counter-balanced by the built-in electric field generated by the fixed charges flanking the junction. As seen in the fixed-charge distribution shown in Figure 1.5c, the space-charge region extends further into the less-conductive n-region, to the point where the net space charges in the n- and  $p^+$ -sides balance. Typical space-charge widths for such a device would extend 1 micron into the n-region, but only 0.1 micron into the  $p^+$ -region. The built-in electric field established by the fixed charge distribution is also indicated in Figure 1.5c. This built-in field is the critical mechanism for separating electron–hole pairs generated under illumination.

When sunlight shines in the vicinity of the  $np^+$  junction, some of the solar photons are absorbed, creating elevated concentrations of electron–hole pairs. Electron–hole pairs generated within or near the space-charge region are separated by the built-in field, with the electrons and holes pushed toward opposite sides of the device. The photocharges successfully extracted are converted to electricity, while the remainder will recombine, losing energy to radiation or heat. Under solar illumination, thermal equilibrium at the junction is disturbed, and a single Fermi level cannot be defined. Instead, quasi-Fermi analysis can be applied, where the original Fermi level splits into separate quasi-Fermi levels for electrons ( $F_e$ ) and holes ( $F_h$ ) [26,27,39,40]. The resulting band diagram for the  $np^+$  junction under illumination at open-circuit conditions is shown in Figure 1.6. Of note, the electron and hole quasi-Fermi levels are continuous across the junction, and converge back to the bulk n-region and p-region levels away from the space-charge region. As a result, the open-circuit potential, represented by the Fermi level offset between the two bulk regions, is determined by the quasi-Fermi level separation in the device.

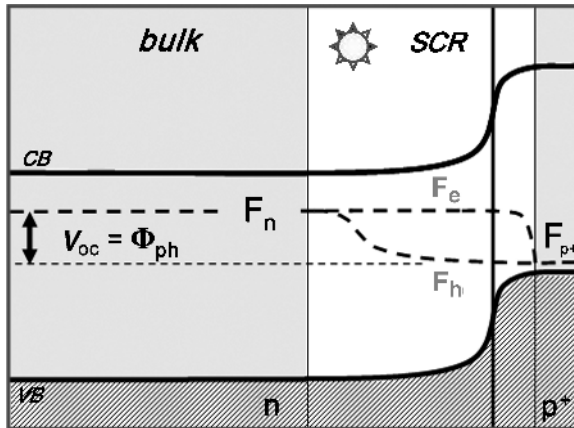


**Figure 1.6** Band diagram of the  $np^+$  junction under solar illumination, illustrating the development of usable photopotential through quasi-Fermi level separation. (SCR stands for space-charge region,  $\Phi_{ph}$  for photopotential,  $V_{oc}$  for open-circuit voltage, and  $F_e$  and  $F_h$  for electron and hole quasi-Fermi levels, respectively).

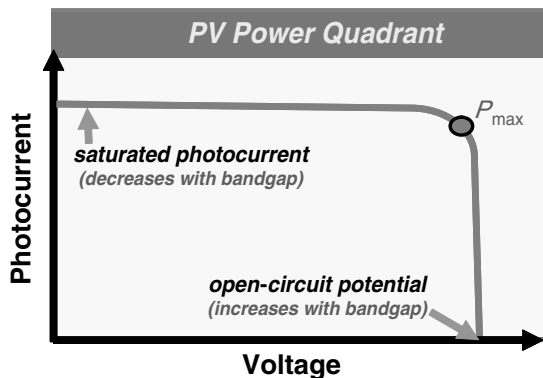


**Figure 1.7** Current–voltage performance curve of solid-state solar cell showing open-circuit potential, the saturated photocurrent level and the maximum power point.

The effect of this quasi-Fermi level split is extremely important to how much *useable* photopotential the device can generate, specifically in relation to the bandgap energy. In crystalline silicon, for example, the bandgap energy is 1.1 eV, while single-junction silicon solar cells have open-circuit voltages typically between 0.6 and 0.7 V. Thermodynamically, semiconductor band-diagram representations reflect the *internal energy* of electrons and holes, not the *useable energy*. Electricity can be extracted from a solar cell at potentials below the open-circuit voltage, which is typically 50–75% of the semiconductor bandgap energy. The output voltage can be increased using higher-bandgap cells, but as a tradeoff, fewer solar-spectrum photons (refer to Figure 1.2) would be absorbed, limiting the saturated photocurrent. The effects of bandgap on photopotential and photocurrent are indicated in the generic solar-cell performance curve of Figure 1.7. These effects remain extremely relevant to the performance of PEC rectifying junctions under sunlight.

### 1.5.3 PEC Junction Formation

To describe rectifying PEC junctions formed at semiconductor/electrolyte interfaces, key principles from solid-state physics and electrochemistry need to be combined. For reference, there is a wealth of literature on fundamental electrochemical principles [41–46], in addition to the previous citations covering semiconductor physics. Of particular interest to PEC studies are the models developed by Gerischer, which make the important connections between the in-solution electrochemical potentials of electrons and solid-state Fermi levels [40,47,48]. Using the Gerischer models, descriptions of semiconductor/electrolyte junctions follow closely the solid-state junction analogies. Photoanodes using n-type semiconductors form PEC junctions similar to an  $np^+$  junction, as depicted in Figure 1.8, while p-type photocathode junction formation, illustrated in Figure 1.9, would be more analogous to a solid-state  $pn^+$  device. Since there are clear symmetries in the development of photoanode versus photocathode junctions, as a starting point it is instructional to focus initially on one, for example the photoanode from Figure 1.8.

Figure 1.8a depicts the photoanode and electrolyte solution before contact. The Fermi level in the n-type semiconductor ( $F_n$ ) is close to the CB, and the Fermi level in solution ( $F_s$ ) falls between the redox (reduction/oxidation) levels for hydrogen reduction ( $H^+/H$ ) and water

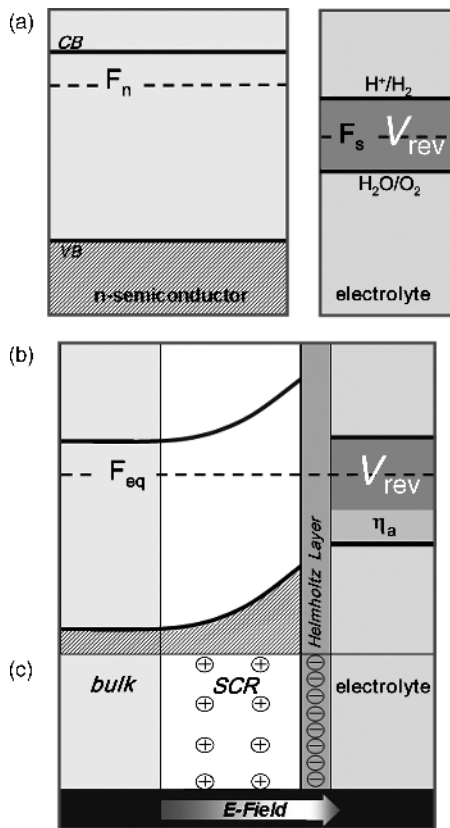


**Figure 1.8** Formation of a semiconductor/electrolyte PEC junction based on an n-type photoanode, showing: (a) semiconductor and electrolyte before contact; (b) band diagram of junction formation and equilibration; and (c) charge distributions in the space-charge region and Helmholtz double layer, and the built-in electric field. ( $F_s$  represents solution Fermi level,  $V_{rev} = 1.23$  eV is the reversible potential for water splitting, and  $\eta_a$  is the anodic overpotential).

oxidation ( $H_2O/O_2$ ). After immersion, the electrode and electrolyte Fermi levels must align to reach thermal equilibrium, as shown in Figure 1.8b. Since the initial electrode Fermi level is higher than the electrolyte Fermi level, free electrons in the n-type semiconductor will migrate to the solid–liquid interface exposing positively charged fixed donor sites, similar to the  $np^+$  example. In the PEC case, however, the electrons form a surface charge layer at the interface, which induces a thin Helmholtz double layer in the electrolyte. The charge distributions including the fixed space charges in the solid-state and the Helmholtz layer charges in solution are shown in Figure 1.8c. Typically, Helmholtz layers are on the order of a few nm, compared with several microns for the semiconductor space-charge region.

As in the  $np^+$  case, electron–hole pairs generated by photon absorption in the space-charge region can be separated by the built-in electric field. Photoexcited electrons are driven toward the electrode’s back contact, where they can be extracted, for example to a counter-electrode in solution. On the other hand, photogenerated holes will be driven toward the interface, where

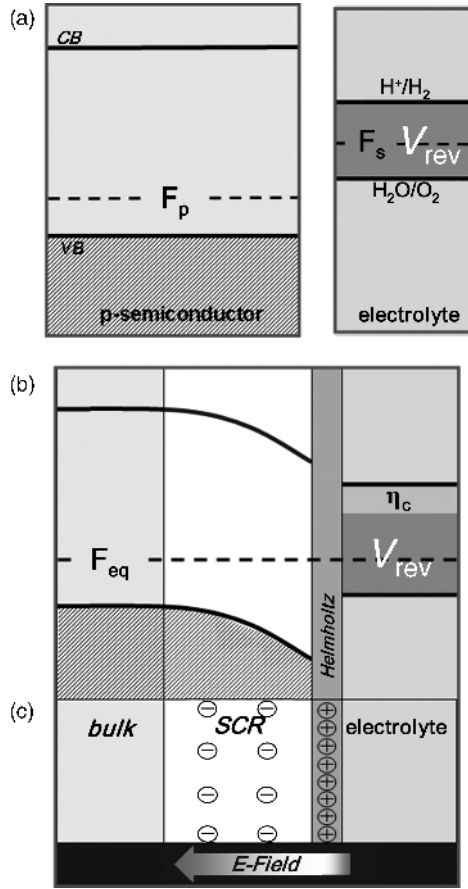


**Figure 1.9** Formation of a semiconductor/electrolyte PEC junction based on a p-type photocathode, showing: (a) semiconductor and electrolyte before contact; (b) band diagram of junction formation and equilibration; and (c) charge distributions in the space-charge region and Helmholtz double layer, and the built-in electric field. (Here,  $\eta_c$  is the cathodic overpotential).

(with the appropriate energetics and kinetics) they can drive oxidation reactions in the electrolyte. Before focusing on the dynamics of the illuminated photoanode, it is worth noting that the equilibrium charge-distribution process is the same for p-type photocathodes, but as shown in Figure 1.9 the charges and band-bending are reversed.

#### 1.5.4 Illuminated Characteristics

Coming back to the photoanode, the PEC junction response to solar illumination is detailed in Figure 1.10. In the figure, the back contact of the photoelectrode is connected by external wiring to a counter-electrode also in solution; and added in the band diagram are  $\eta_a$  and  $\eta_c$ , the overpotentials for water oxidation and hydrogen reduction associated with photoanode and counter-electrode interfaces, respectively. With the addition of sunlight, there is again

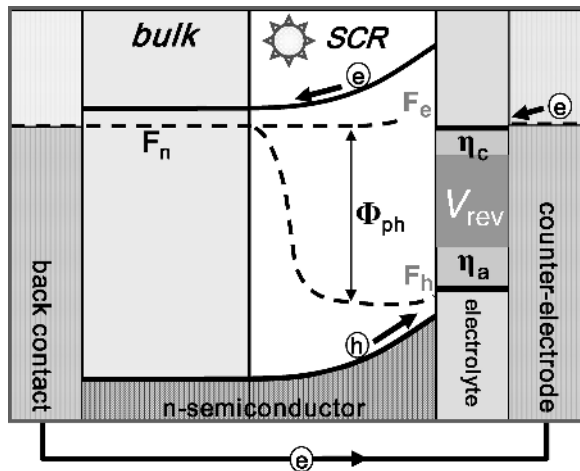


**Figure 1.10** Band diagram of the photoanode PEC junction under solar illumination, illustrating the development of sufficient photopotential (i.e., quasi-Fermi-level split) to overcome the reversible potential plus the anodic and cathodic overpotentials for water splitting.

a quasi-Fermi-level split resulting from the excess concentration of photogenerated electron–hole pairs. With respect to the thermal equilibrium populations of carriers, the excess hole population significantly alters the minority-carrier distribution, while the excess electrons barely affect the majority-carrier numbers. As a result, the hole quasi-Fermi level shifts substantially in contrast to insignificant change in the electron quasi-Fermi level.

As in the solid-state case, the quasi-Fermi separation determines the *useable* energy in the device. In Figure 1.10, the electron potential at the counter-electrode, tied to the photoanode’s back contact potential, is sufficiently high to drive the hydrogen-reduction half-reaction (including  $\eta_c$ ). Simultaneously, the quasi-Fermi hole energy at the solution interface is sufficiently *low* to drive water-oxidation (including  $\eta_a$ ). In consequence, this configuration is capable of sustaining the net PEC water-splitting process, driven by *useable* energy in the quasi-Fermi split (*not* by the *internal* energy in the bandgap.). It is often misreported that semiconductors with bandgaps “straddling” the redox potentials can photosplit water. Counter examples are illustrated in Figures 1.11 and 1.12. In both cases the conduction and valence-band edges clearly straddle the redox levels, including the overpotentials. In Figure 1.11, however, the hole quasi-Fermi level at the PEC interface is too high, while in Figure 1.12, the electron potential in the counter-electrode is too low. In either case PEC water splitting is not sustainable. An interesting variation to Figure 1.12 is seen in Figure 1.13: an external voltage source has been added between the photoanode and counter-electrode, boosting electron energies enough to support the hydrogen reduction. This can split water, but no longer qualifies as a simple solar-to-hydrogen conversion process.

### 1.5.5 Fundamental Process Steps

From the previous examples, it becomes evident that high-bandgap semiconductors are needed just to meet the energetic requirements for single-junction PEC water splitting.

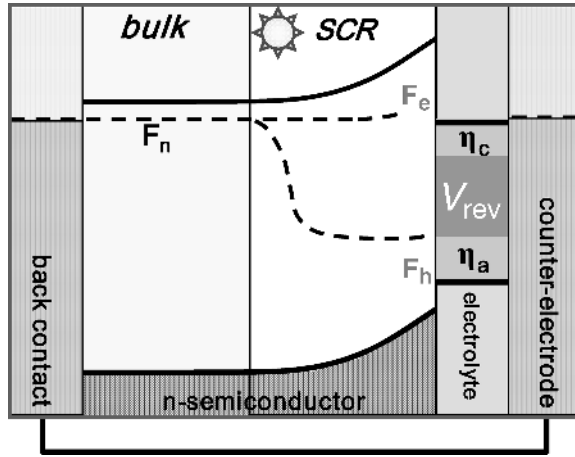


**Figure 1.11** Non-operational photoanode junction with insufficient  $F_h$  for driving the water oxidation half-reaction.

As in the solid-state case, a large bandgap increases the photopotential, but also reduces the photocurrent. This is particularly unfortunate, since hydrogen production rates and STH conversion efficiencies, as shown in Equations 1.2 and 1.3, are directly proportional to the photocurrent. Quantitative effects of this current–voltage tug-of-war will be evident in some real-world examples of single-junction PEC water splitting. Beforehand, to focus on the important performance-limiting loss mechanisms, it’s worth reviewing the

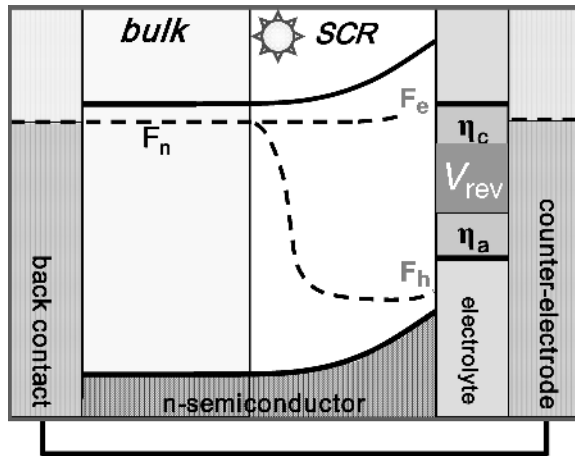


**Figure 1.12** Non-operational photoanode junction with insufficient  $F_e$  for driving the hydrogen reduction half-reaction.

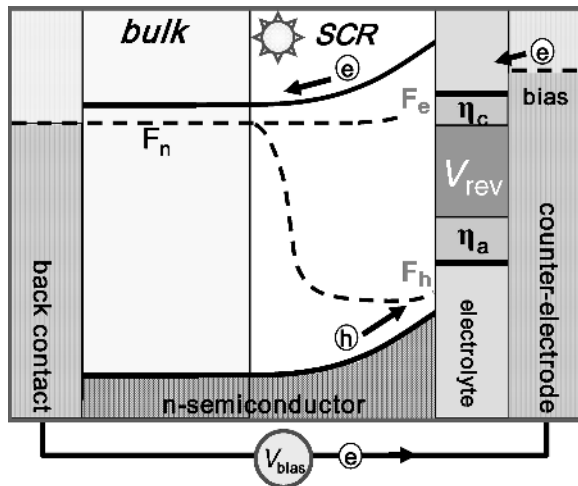


**Figure 1.13** Addition of an external bias to the photoanode configuration shown in Figure 1.12, in effect raising the counter-electrode electron energy to enable PEC water-splitting.

fundamental solar-to-hydrogen process steps specifically applied to single-junction photo-electrode systems:

1. **Photon-Absorption and Charge Generation:** In single-junction absorbers, photons with energies below the semiconductor bandgap cannot be absorbed or converted. Photons with energies exceeding the bandgap are absorbed at rates dependent on the allowed transitions in the semiconductor. Direct bandgap materials absorb more efficiently than indirect bandgap materials. Photogenerated electron–hole pairs rapidly thermalize (usually within picoseconds) to band-edge energy levels, losing energy to heat. High-bandgap semiconductors generate little photocurrent due to poor absorption, while low bandgap semiconductors can suffer from low conversion efficiency due to high thermalization losses.
2. **Charge Separation and Transport:** While at band-edge energy states, the electron–hole pairs can often survive for several microseconds before recombining. During this time, they must be separated and transported to electrochemical interfaces for extraction. This separation is assisted by the electric fields set up by charge distributions in the semiconductor and at the solid/liquid interface. Defects in the bulk and at the interface can adversely affect the separation fields, and also result in poor mobility for charge transport. If wide absorption widths are needed (for example, in indirect semiconductors) the charge transport losses can be severe.
3. **Charge Extraction/Electrochemical Product Formation:** Ideally, charge is extracted via the water splitting half-reaction at the solid/liquid interface. The extraction process can be slowed or completely inhibited by poor energetic alignment or poor surface kinetics at the photoelectrode or counter-electrode surfaces. Moreover, parasitic or corrosion reactions competing with the water-splitting reactions can result in substantial loss. Surface treatments can be employed to kinetically and/or energetically favor water splitting over the parasitic processes, but such treatments could also block sunlight. Surface incorporation of nanoparticle catalysts is one approach. Since PEC water splitting is a low-current-density

process (typically operating below  $20 \text{ mA cm}^{-2}$ ), non-precious-metal catalysts can be used. Additionally, nanostructuring of electrode surfaces can increase effective surface area for enhanced charge extraction, although this can also lead to higher surface recombination loss. On the solution side, the electrolyte is an important factor determining stability, efficiency of the charge-extracting reactions, and the electrochemical byproducts. Splitting seawater, for example, is a challenge, since it is difficult to electrochemically suppress the production of chlorine gas from the  $\text{Cl}^-$  ions [49].

- 4. Electrochemical Product Management:** During PEC water splitting, the evolved hydrogen or oxygen gas must be efficiently removed from the photoelectrode surface to avoid mass-transport losses in the surface reactions, and to minimize adverse optical effects. Surfactants added to the electrolyte have been successful in promoting rapid bubble formation and dissipation. In solution, ionic conductivity losses tend to be a bigger problem. High electrolyte concentrations can be used to minimize this loss, but the tradeoff is in higher corrosivity. Photoelectrode geometry and counter-electrode proximity are critical parameters to the redistribution of ions. In some geometries, gas-separating membranes are needed, introducing further ionic-transport loss.

## 1.6 Photoelectrode Implementations

### 1.6.1 Single-Junction Performance Limits

With inherent electrochemical and solid-state losses, it is difficult to achieve high STH conversion efficiencies in single-junction PEC photoelectrode systems. The bandgap tradeoff between photopotential and photocurrent is particularly detrimental for single junctions. For example, if the minimum water-splitting potential (based on redox separation with overpotentials) amounts to 1.6 eV, and the quasi-Fermi-level separation in the semiconductor can achieve 50% of the bandgap level, then the minimum bandgap for the onset of photoelectrolysis would be 3.2 eV. For any appreciable level of hydrogen production, overpotential and other system losses increase, requiring even higher bandgaps.

How efficient would such high-bandgap single junctions be? It is easy to establish an upper bound based on optical absorption limits. Figure 1.14 plots the maximum attainable AM1.5<sub>global</sub> photocurrent densities in a semiconductor as a function of bandgap. The derivation assumes that every photon in the solar spectrum with an energy exceeding the bandgap will create an electron-hole pair, and that all of these electron-hole pairs are converted to photocurrent. For bandgaps greater than 3.2 eV, photocurrent density is limited to approximately  $1 \text{ mA cm}^{-2}$ . This, according to Equation 1.3, places an upper STH efficiency limit of 1.23%. STH values based on Equation 1.3 are listed in parentheses on the right vertical axis of the Figure 1.14, but these only apply to standalone configurations capable of water splitting. For any bandgap, if the photoelectrode system cannot sustain photoelectrolysis, there is no photocurrent density, and the conversion efficiency is 0% STH.

To date, the only demonstrations of single-junction water splitting have utilized very-high-bandgap materials, such as  $\text{SrTiO}_3$  and  $\text{KTaO}_4$  [50,51]. Based on poor photon absorption, the demonstrated STH values have been very small, consistent with the predictions in Figure 1.14. Also indicated in this figure are the bandgap positions for polycrystalline  $\text{Fe}_2\text{O}_3$ ,  $\text{WO}_3$  and  $\text{TiO}_2$ , three commonly studied in PEC materials. The potential photocurrent densities look encouraging, especially for iron oxide, but none of these materials develop enough

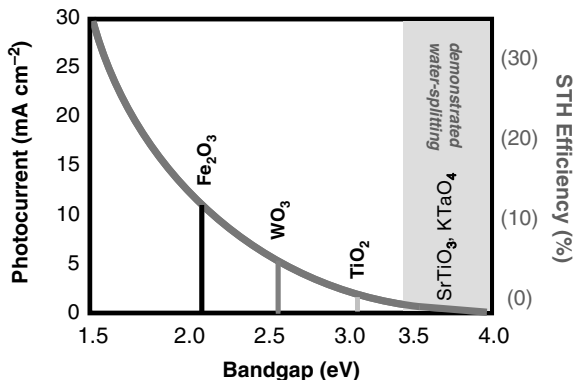


**Figure 1.14** Maximum attainable AM1.5<sub>global</sub> photocurrent densities (in mA cm<sup>-2</sup>) for single-junction PEC devices shown as a function of semiconductor bandgap. Also shown are the corresponding STH efficiencies applicable only to operational water-splitting junctions.

photopotential under sunlight to split water, not even TiO<sub>2</sub>, with a bandgap over 3.0 eV. To enhance the photopotential, these and other promising semiconductors can be incorporated in multijunction PEC schemes.

### 1.6.2 Multijunction Performance Limits

Multijunction devices are well-known in the PV community. In fact, the use of multiple junctions to improve the solar-to-electricity conversion efficiency is one of the cornerstones of *third generation research* [52]. For PEC devices, a similar approach can be taken to enhance photopotential and increase absorption efficiency in a PEC. The concept is illustrated in Figure 1.15 for a two-junction (tandem) system. Sunlight is partly absorbed in the higher-bandgap top junction, while the remaining filtered light is absorbed in the lower-bandgap bottom junction. Both junctions generate photovoltage and photocurrent. Since they are stacked in a series-connected configuration, the photovoltages  $V_1$  and  $V_2$  will add, but the photocurrents will not. In fact, the net photocurrent will be the minimum of  $J_1$  and  $J_2$ , which is the bottle-neck for current flow across the device. For optimal performance, it is therefore critically important to current-match  $J_1$  and  $J_2$  by optical tuning of the two junctions.

In PEC water-splitting applications, multiple junctions can be stacked to take advantage of the photopotential enhancement. The tradeoff is reduced photocurrent, which directly limits hydrogen production rates. The device design must strike the right balance to maximize conversion efficiency. Two different design approaches using tandem junctions to photosplit water are shown in Figure 1.16. Figure 1.16a depicts a PEC/PEC tandem [53], where a photoanode and photocathode, both deposited onto transparent substrates, are stacked one in front of the other, and electrically connected by a wire. The configuration in Figure 1.16b represents a PEC/PV hybrid electrode [1,54–56], with a PEC top junction monolithically stacked with a solid-state PV bottom junction, and connected to a counter-electrode. Both designs have their own merits and disadvantages. The PEC/PV tandem entails extra fabrication complexity, but takes advantage of synergies with PV technology. Many good device-quality thin-film PV materials are available for the bottom cell, so the challenge is to develop a

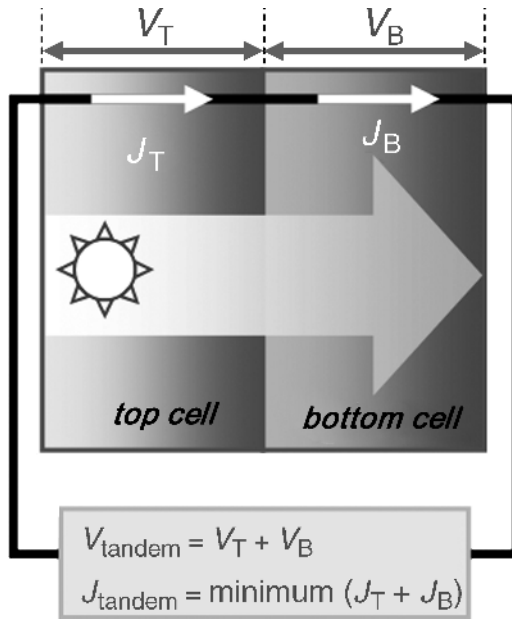


**Figure 1.15** Block diagram of a stacked, series-connected tandem device under solar illumination. Photocurrents,  $J$ , and photovoltages,  $V$ , are shown for the top cell, the bottom cell and the combined tandem device.

compatible PEC material for the top junction. The PEC/PEC tandem has better potential for low-cost electrode synthesis, but involves external interconnections and requires development of two PEC materials (as if one wasn't enough!). The real bottom line will rest with actual relative device performance in the different tandem configurations.

As with the single-junction cases, efficiency bounds can be placed on such tandem configurations based on optical absorption limits. Figure 1.17 is essentially a two-dimensional extension of Figure 1.15 for tandem devices, where maximum photocurrent and the corresponding STH levels are calculated as a function of both top- and bottom-junction bandgaps. The assumptions are as follows: (1) the top cell absorbs all photons with energies exceeding the top-cell bandgap; (2) the bottom cell is illuminated with the top-cell-filtered light, and absorbs all of the remaining photons with energies exceeding its bandgap; (3) photocurrent density (in  $\text{mA cm}^{-2}$ ) is calculated based on the minimum electron-hole pair count from the two junctions, assuming all of these pairs are converted to current; and (4) STH efficiencies, shown in parentheses, are calculated using Equation 1.3, and only apply to systems with sufficient photopotentials to split water.

The numbers from Figure 1.17 are definitely encouraging for the viability of tandem PEC hydrogen production. Despite the split spectrum and reduced photocurrents, a wide range of bandgap combinations yield high enough photocurrents for  $>10\%$  STH conversion. An important key is to identify the possible combinations capable of the necessary photopotential levels. A quick-and-dirty rule of thumb can be derived based on typical quasi-Fermi level splits, for example about 50% of the bandgap for many semiconductors under solar illumination: the average of the top- and bottom-cell bandgaps needs to exceed the water-splitting potential, including the overpotentials, for example around 1.6 eV in typical

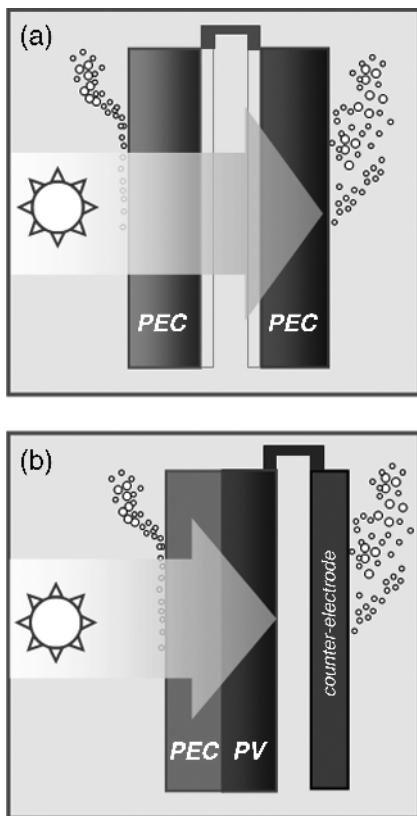


**Figure 1.16** Design configurations for PEC water-splitting tandem devices showing: (a) a PEC/PEC photoanode/photocathode tandem with the two electrically connected photoelectrodes fabricated on transparent substrates for light transmission; and (b) a hybrid PEC/PV monolithically stacked device connected to a counter-electrodes.

photoelectrode configurations. There are many pitfalls and extra losses in real-world multijunction implementations, so this *rule* is by no means a guarantee of success. It is, however, quite useful in brainstorming sessions about device design.

As an illustration,  $\text{TiO}_2$  with bandgaps of 3.1 eV could be combined with a low-bandgap semiconductor such as silicon (1.1 eV) in a hybrid tandem to meet the photopotential requirement for PEC water-splitting. As seen in Figure 1.17, however, independent of the bottom junction, the device performance will never exceed 5% STH. In this, and any series-connected tandem configuration, the performance is bound by the photocurrent limits of the PEC semiconductor. To achieve STH efficiencies above 10%, we can start back at Figure 1.14 and select semiconductors with bandgaps less than 2.2 eV for a top cell. For an average exceeding 1.6 eV, the bottom cell must be at least 1.0 eV. Using Figure 1.17, STH just straddles the 10% mark for bottom-cell bandgaps ranging from the 1.0 eV minimum up to 1.7 eV. The bandgaps should be somewhat lower than 2.2 eV for the top cell, and correspondingly higher than 1.0 eV in the bottom cell for more robust hydrogen production rates. In fact, such a device has already been designed, fabricated and successfully demonstrated in the laboratory.

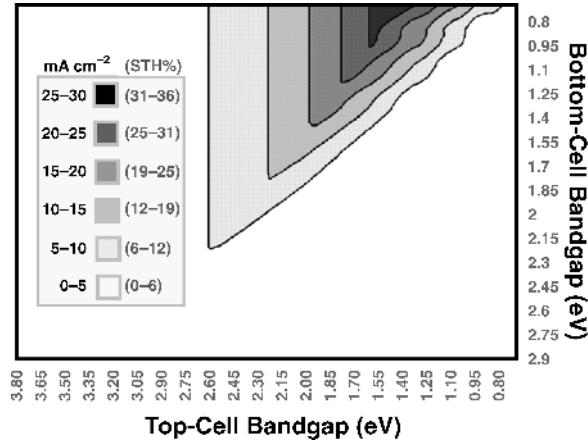


**Figure 1.17** Maximum attainable AM1.5<sub>global</sub> photocurrent densities (in mA cm<sup>-2</sup>) for tandem PEC devices shown as a function of top-cell and bottom-cell bandgaps. Also shown are the corresponding STH efficiencies applicable only to operational water-splitting devices.

*1.6.3 A Shining Example*

The NREL, using a multijunction hybrid photoelectrode, holds the STH efficiency world record for PEC water splitting [1]. The hybrid tandem device incorporates high-quality III–V crystalline semiconductor materials, with a 1.44 eV GaAs PV junction as the bottom cell, and a 1.83 eV Ga-InP PEC junction as the PEC top cell. As seen in Figure 1.18, this is a tandem photocathode configuration, where hydrogen is evolved at the PEC interface and oxygen is evolved at the separated counter-electrode. As seen in the device band diagram representation in Figure 1.19, there is a characteristic downward band-bending at the solid/liquid interface, consistent with the photocathode formulation in Figure 1.9. Tracking the combined quasi-Fermi level splits across the tandem, it can be seen that sufficient photopotential is developed to

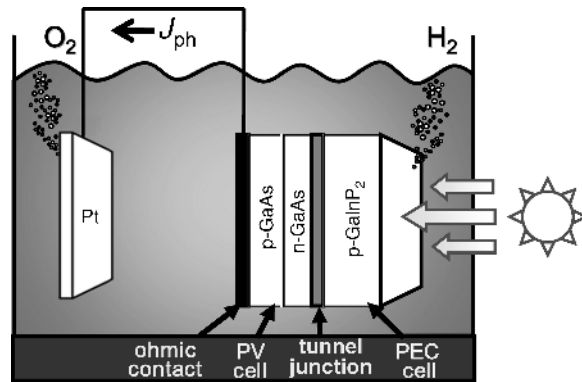


**Figure 1.18** Two-electrode setup for the NREL hybrid PEC/PV photocathode demonstrating a 16% world-record STH efficiency.

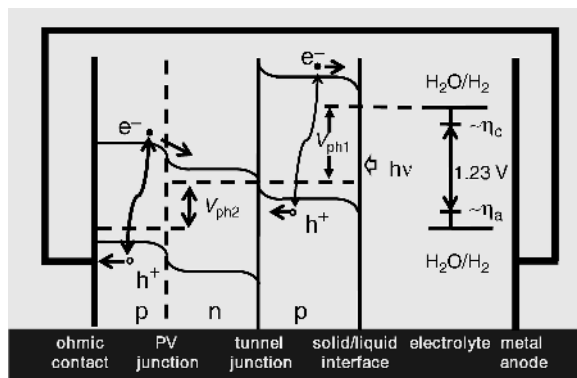


**Figure 1.19** Band diagram of the PEC water-splitting process in the NREL tandem photocathode implemented in a two-electrode configuration.

drive both the hydrogen-reduction and water-oxidation reactions. Cross-referencing the top- and bottom-cell bandgaps in Figure 1.17, we would expect a solar-to-hydrogen conversion efficiency in the 10–20% range. In fact, this tandem device has demonstrated an astounding 16% STH efficiency! This laboratory-scale device is fabricated using extremely expensive III–V materials (the kind only NASA can afford!) and suffers from limited durability, it's not quite the grail. Still, the NREL hybrid tandem remains the best shining example of *what PEC can achieve*.

## 1.7 The PEC Challenge

### 1.7.1 What's Needed, Really?

In a nutshell, can the PEC performance levels of the NREL tandem device be reproduced using low-cost, high-durability devices and systems? The usual suspects under investigation for decades, including particulate and thin-film forms of metal oxides such as  $\text{TiO}_2$ ,  $\text{WO}_3$  and  $\text{Fe}_2\text{O}_3$ , haven't been able to cut it in the performance category. In fact, the best-demonstrated STH efficiencies in these materials, achieved using  $\text{WO}_3$  in multijunction photoanode devices, has plateaued in the 3–5% range for quite some time [3,4].

Breakthroughs are needed, on several fronts: new particulate or thin-film semiconductor materials with good absorption and carrier-transport properties need to be developed; and novel interfaces need to be designed with energetic and kinetic properties favoring the water-splitting reactions, and inhibiting corrosion reactions. Even with these breakthrough materials and interfaces, very clever integrated devices need to be devised and manufactured using low-cost, commercial-scale processes. Many stars must align before mastering that delicate balancing act of PEC hydrogen production. In summary, the holy grail PEC system will be held to the following decrees:

- **Thou shall generate sufficient photopotential to split water.** In other words, the net quasi-Fermi level split must be large enough to overcome the reversible potential plus the overpotentials for water-splitting, typically over 1.6 eV in practical systems.

- **Thou shall generate sufficient photocurrent for efficient hydrogen production.** In other words, semiconductor and solution properties, in addition to the interface energetics and kinetics, must support the efficient generation, separation, transport and collection of photogenerated charges to drive the water-splitting reactions. Photocurrents exceeding  $10 \text{ mA cm}^{-2}$ , for example, are needed for STH conversion efficiencies over 12.3%.
- **Thou shall not corrode.** High hydrogen production rates must be sustained over long durations with minimal corrosion and degradation. Interface energetics/kinetics must favor water-splitting reactions over corrosion reactions.
- **In the long term, Thou shall cost next to nothing!**

### 1.7.2 Tradeoffs and Compromises

Again, this is not an easy task. In efforts to achieve practical PEC hydrogen production, tradeoffs abound and compromises are many. Cost versus performance will remain the central tradeoff in PEC research pending major breakthroughs in materials and interfaces. In the meantime, researchers remain preoccupied searching for pathways forward, based on the right compromises along numerous avenues. The fundamental photocurrent/photovoltage tradeoff will not go away, but pathways around this are available, including multijunctions and further down the road, hot-carrier collection [52,57,58]. The basic implementation of PEC semiconductors in commercial hydrogen production plants has not been settled. What are the tradeoffs between large-scale photoelectrode reactors (e.g., panel- or tubular- types) using low-cost thin-film materials and large-scale slurry-bed reactors utilizing functionalized semiconductor particles [59]. Assuming the right thin-film or particulate materials can be found, more techno-economics analyses will be needed to resolve this debate. The path forward needs to navigate all the economic, as well as the scientific obstacles.

### 1.7.3 The Race with PV-Electrolysis

If the PEC holy grail is found, how would it stack up against, for example, PV-electrolysis systems for hydrogen production? At first glance, PEC might look pretty good next to PV-electrolysis. Take for example what a *low-cost* PV-electrolysis system might look like today. A *relatively cheap* 10% amorphous silicon PV system coupled with a 60% PEM electrolyzer gives us only 6% STH. Higher-cost more-efficient components are available, but in the *low-cost/high-performance* race, much R&D is needed here as well. Interestingly, the semiconductor materials research efforts in PV and PEC are highly synergistic, and breakthroughs in either can greatly benefit both. The real race is toward the practical solar production of hydrogen from water, no matter how we get there, everyone wins!

## 1.8 Facing the Challenge: Current PEC Materials Research

Across the United States and around the world, the latest and greatest scientific advances are being brought to the table to face the PEC challenge. Key patrons in the quest include the US Department of Energy's (DOE) Working Group on PEC Hydrogen Production [60], and the International Energy Agency's Hydrogen Implementation Agreement (IEA-HIA) [61]. In recent years, powerful synergies developed in the PEC community have become infectious, drawing together researchers from diverse fields, including photovoltaics, nanotechnology and

the *other* solar-hydrogen routes. Globally, *renewable hydrogen* research is getting some new life, as evidenced in numerous recent publications, including several informative books [62,63]. There is an important unifying theme linking all renewable-energy research fields, including PEC hydrogen, and that theme is *materials, materials, materials!*

Fundamental materials and materials-interface properties hold the keys to successful PEC research and development. In response, the worldwide PEC network is constructing a specialized “tool-chest”, including state-of-the art techniques in materials theory, synthesis and characterization, to facilitate research progress, and to help inspire fundamental breakthroughs. This tool-chest is already proving invaluable in the investigation of promising PEC semiconductors and interfaces. As collaborative activities expand, it is expected to become an even more powerful asset.

To foster collaboration, the DOE PEC Working Group and the IEA-HIA PEC Annex-26, are encouraging the formation of informal international “task forces” to coordinate important PEC research activities. While some of the collaborative task forces center on the R&D of specific PEC materials classes, others focus on critical activities to advance the supporting science and technologies in the PEC tool-chest. These include:

- Development of standardized testing and reporting protocols for evaluating candidate PEC materials systems on a level playing field. In the past, the lack of standardized conditions and procedures for reporting PEC results has greatly hampered research progress across the board [64].
- Development of advanced characterization techniques to enhance understanding of PEC materials and interfaces, and promote breakthrough discoveries [65]. The most advanced methods in evaluating optoelectronic properties of semiconductor materials and interfaces, *in situ* as well as *ex situ*, are being deployed.
- Development of new theoretical models of PEC materials and interfaces critical to the design and engineering of brand new semiconductor systems [66,67]. Sophisticated models of band states and bandgaps are needed, including effects of surface, interfaces and grain boundaries.
- Development and implementation of innovative synthesis techniques, including combinatorial synthesis methods, to facilitate the PEC materials discovery process [68,69]. Innovative synthesis routes can make or break the viability of a semiconductor system, a fact well-appreciated by the PV community.
- Development and refinement of *techno-economics analyses* of PEC hydrogen-production systems incorporating performance and processing-cost feedback from the broader materials R&D efforts. This will provide a basis for evaluating the long-term feasibility of large-scale PEC production technologies in comparison with other renewable approaches.

On an impressive scale, the PEC research community is applying its tool-chest to investigate a broad spectrum of promising materials classes. Some of the materials task forces are concentrating on modification of traditional materials, others are focusing on more practical synthesis approaches for expensive, high-performance materials, and yet others are attempting to discover completely new material systems. For all of the different materials, task-force researchers must carefully consider the benefits, barriers and approaches for addressing the barriers; all in close coordination with the ongoing advances in theory, synthesis and characterization. Some of the important PEC materials classes under current investigation worldwide include:

- **Tungsten-oxide and related modified compounds:** Tungsten oxide, particularly in thin-film and nanoparticle forms, has been a workhorse in photoelectrochemical [70–73] and electrochromic [74] applications for years. It is inexpensive and stable, but its high bandgap ( $\sim 2.6$  eV) is limiting to PEC performance. Photocurrent densities around  $3 \text{ mA cm}^{-2}$  have been achieved [4,75,76], with STH efficiencies over 3% in tandem configurations. To break the performance barrier, current research is focused on reducing bandgap through ion incorporation into the  $\text{WO}_3$  structure [66,67,77], and further integration in multijunction devices.
- **Iron-oxide and related modified compounds:** Iron-oxide is abundant, stable, inexpensive and has a near-ideal bandgap ( $\sim 2.1$  eV) for PEC applications. Unfortunately, its poor absorption, photocarrier lifetime and transport properties have been prohibitive to practical water splitting. Current research to overcome these barriers has been encouraging, with recent progress in thin films [78–81] and nanostructured materials [82]. Iron oxide in tandem configurations may also be of interest.
- **Amorphous silicon compounds, including silicon carbides and nitrides:** Amorphous silicon compounds have recently demonstrated interesting performances in PEC applications [56,83–87]. The progress of this material class in photoelectrochemical applications has benefited from decades of research in the PV community. Technical barriers remain in PEC stability and interface properties, but electrolyte and surface modification studies could help overcome these barriers. With material and interface improvements, monolithically fabricated multijunction devices using amorphous silicon compound films can have practical appeal for PEC water-splitting.
- **Copper chalcopyrite compounds:** Copper chalcopyrite thin films are among the best absorbers of solar energy. As a result, chalcopyrite alloys formed with copper and gallium, indium, sulfur and selenium have been widely characterized in the PV world [88,89]. A great advantage of this material class for PEC applications is the bandgap tailoring based on composition, with bandgaps ranging from 1.0 eV in  $\text{CuInSe}_2$  to 1.6 eV in  $\text{CuGaSe}_2$ , and up to 2.43 eV in  $\text{CuGaS}_2$  [90]. The  $\text{CuGaSe}_2$  bandgap is attractive for PEC applications, and photocurrent density exceeding  $13 \text{ mA cm}^{-2}$  have been demonstrated with this material [91] in biased PEC cells. Stability, surface kinetics and surface energetics remain as current barriers, but if current research can successfully address these, high STH efficiency could be achievable in low-cost thin-film copper chalcopyrite systems.
- **Tungsten and molybdenum sulfide nanostructures:** As bulk materials, tungsten and molybdenum sulfides are excellent hydrogen catalysts, but their bandgaps (below 1.2 eV) are too low for PEC water splitting. Quantum confinement using nanostructuring, however, can increase the bandgap up to 2.5 eV. Current studies on nanostructured  $\text{MoS}_2$  are focused on stabilized synthesis routes and integration of the nanostructures into practical bulk PEC devices [92].
- **III–V semiconductor classes:** High-quality crystalline semiconductor compounds of gallium, indium, phosphorous and arsenic have been studied for decades [93]. In PEC experiments to date, STH efficiencies between 12–16% have been demonstrated in  $\text{GaInP}_2/\text{GaAs}$  hybrid tandem photocathodes [1,94]. High cost and limited durability are the barriers to practical PEC hydrogen production, and breakthroughs in synthesis and in surface stabilization are being pursued.

Although there is still much work ahead, research in these promising candidate materials, among others, has seen significant recent progress. Fortunately, in today's broad-based

network of PEC collaborators, progress in any one area can greatly benefit all. The needed scientific breakthroughs are still on the way, but once they get here, watch out! The implications of new low-cost, high-efficiency semiconductors will be enormous, not only to PEC solar water splitting for hydrogen production, but also to PV and other solar-energy conversion pathways. The challenge is great, but the promise even greater.

## Acknowledgments

First, I would like to applaud the worldwide network of PEC researchers who carry out the quest with such dedication and enthusiasm, and would like to thank especially all participants in the US DOE PEC Working Group and of the IEA-HIA PEC Annex-26 for their excellent work and fruitful collaborative efforts. This list is long, and it includes (but is by no means limited to) the following: my good friend Dr. Clemens Heske and his excellent cohorts at UNLV; Dr. Arun Madan and his incredibly dedicated research team at MVSystems Incorporated; Dr. Eric McFarland and his amazing pool of talented students at UCSB; the brilliant Dr. Tom Jaramillo and his brand new laboratory at Stanford; and of course Drs. John Turner, Mowafak Al-Jassim, Todd Deutsch, Huyen Dinh and all the other superb NRELians! My sincere appreciation and gratitude goes out to the Hawaii Natural Energy Institute (HNEI) at the University of Hawaii at Manoa; Its director Dr. Richard Rocheleau and excellent staff, including Dr. Michael Antal, Dr. Bor Yann Liaw and Mitch Ewan have been instrumental in the advancement of hydrogen and renewable Energy. My very special thanks go out to all researchers and assistants, past and present, of the HNEI Thin Films Laboratory (TFL) who have carried the PEC torch with dignity and grace for many years From the recent past, Drs. Bjorn Marsen, Brian Cole and Daniela Paluselli have made significant contributions; The current TFL staff of Dr. Nicolas Gaillard, Jess Kaneshiro, Alex DeAngelis, Xi Song and Stewart Mallory will have my eternal gratitude, not only for their good work, but also for their tireless efforts in the preparation of this chapter. I would like to send a special Mahalo to Mary-Rose Valladares and Andreas Luzzi of the IEA, and Richard Farmer and David Peterson of the US DOE for their invaluable support of PEC research. Finally, I humbly give my thanks and Aloha to Dr. Robert Perret of Nevada Technical Services, LLC, and Roxanne Garland of the US DOE for their vision, inspiration, and unwavering moral support!

## References

- [1] Khaselev, O., Bansal, A. and Turner, J.A. (2001) High-efficiency integrated multijunction photovoltaic/electrolysis systems for hydrogen production. *International Journal of Hydrogen Energy*, **26**, 127–132.
- [2] Andreev, V.M. (2003) *Practical Handbook of Photovoltaics: Fundamentals and Applications* (eds T. Markvart and L. Castañer), Elsevier.
- [3] Grätzel, M. (2001) Photoelectrochemical Cells. *Nature*, **414**, 338.
- [4] Marsen, B., Miller, E.L., Paluselli, D. and Rocheleau, R.E. (2007) Progress in sputtered tungsten trioxide for photoelectrode applications. *International Journal of Hydrogen Energy*, **32**, 3110–3115.
- [5] Bush, G.W. (January 2003) State of the Union. Presented in Washington, D.C.
- [6] Romm, J.J. (2004) *The Hype About Hydrogen*, Island Press.
- [7] Ball, M. and Wietschel, M. (2009) *The Hydrogen Economy: Opportunities and Challenges*, Cambridge Press.
- [8] Rifkin, J. (2003) *The Hydrogen Economy*, Tarcher.
- [9] Yürüm, Y. (1995) *Hydrogen Energy System: Production and Utilization of Hydrogen and Future Aspects*, Kluwer Academic Publishers.

- [10] Turner, J.A. (1999) A realizable renewable energy future. *Science*, **285**, 687–689.
- [11] Newton, J. (1989) *Uncommon Friends: Life with Thomas Edison, Henry Ford, Harvey Firestone, Alexis Carrel, & Charles Lindbergh*, Mariner Books.
- [12] US Department of Energy, Office of Science (2005) Basic Research Needs for Solar Energy Utilization.
- [13] Green, M.A. (1982) *Solar Cells: Operating Principles, Technology, and System Applications*, Prentice-Hall, Inc.
- [14] US Department of Energy, Energy Information Administration (2008) International Energy Outlook 2008 (DOE/EIA-0484).
- [15] Greentech Media, the Prometheus Institute (2008) PV Technology, Production and Cost, 2009 Forecast: The Anatomy of a Shakeout.
- [16] Solarbuzz (2009) Marketbuzz 2009: Annual World Solar PV Market Report. San Francisco, CA.
- [17] Emery, K. (2003) *Handbook of Photovoltaic Science and Engineering* (eds A. Luque and S. Hegedus), John Wiley & Sons, Ltd.
- [18] Sandia National Laboratories (2008) Sandia Stirling Energy Systems set new world record for solar-to-grid conversion efficiency. Press Release. 2 Feb. 2008.
- [19] CSP Project Developments in Spain (2002) *IEA SolarPACES Implementing Agreement*. <http://www.solarpaces.org/News/Projects/Spain.htm>.
- [20] Kasahara, S., Hwang, G.J., Nakajima, H. *et al.* (2003) Effects of process parameters of the IS process on total thermal efficiency to produce hydrogen from water. *Journal of Chemical Engineering of Japan*, **36**, 887–889.
- [21] Onuki, K., Inagaki, Y., Hino, R. and Tachibana, Y. (2005) Research and development on nuclear hydrogen production using HTGR at JAERI. *Progress in Nuclear Energy*, **47**, 496–503.
- [22] Lewis, M.A., Serban, M. and Basco, J.K. (2004) A progress report on the chemistry of the low temperature Cu-Cl thermochemical cycle. *Transactions of the American Nuclear Society*, **91**, 113–114.
- [23] Akkerman, I., Janssen, M., Rocha, J. and Wijffels, R.H. (2002) Photobiological hydrogen production: photochemical efficiency and bioreactor design. *International Journal of Hydrogen Energy*, **27**, 1195–1208.
- [24] Zaborsky, O.R. (1998) *Biohydrogen*, Plenum Press.
- [25] Funk, J.E. and Reinstrom, R.M. (1966) Energy requirements in production of hydrogen from water. *Industrial & Engineering Chemistry Process Design and Development*, **5**, 336–342.
- [26] Sze, S.M. (2006) *Physics of Semiconductor Devices*, John Wiley and Sons, New York.
- [27] Neamen, D.A. (2002) *Semiconductor Physics and Devices: Basic Principles*, McGraw-Hill Science/Engineering/Math.
- [28] Marcus, R.J. (1965) Chemical conversion of solar energy. *Science*, **123**, 399–405.
- [29] Bockris, J.O.M. (1956) Kinetics of activation controlled consecutive electrochemical reactions: anodic evolution of oxygen. *Journal of Chemical Physics*, **24**, 817–827.
- [30] Dutta, S. (1990) Technology assessment of advanced electrolytic hydrogen production. *International Journal of Hydrogen Energy*, **15**, 379–386.
- [31] LeRoy, R.L. (1983) Industrial water electrolysis: present and future. *International Journal of Hydrogen Energy*, **8**, 401–417.
- [32] Parkinson, B. (1984) On the efficiency and stability of photoelectrochemical devices. *Accounts of Chemical Research*, **17**, 431–437.
- [33] Dohrmann, J.K. and Schaaf, N.S. (1992) Energy conversion by photoelectrolysis of water: determination of efficiency by *in situ* photocalorimetry. *The Journal of Physical Chemistry*, **96**, 4558–4563.
- [34] Heller, A. (1982) Electrochemical solar cells. *Solar Energy*, **29**, 153–162.
- [35] Khan, S.U.M., Al-shahry, M. and Ingler, W.B. Jr. (2002) Efficient photochemical water splitting by a chemically modified n-TiO<sub>2</sub>. *Science*, **297**, 2243–2245.
- [36] Luther, J. (2003) *Handbook of Photovoltaic Science and Engineering* (eds A. Luque and S. Hegedus), John, Wiley & Sons Ltd.
- [37] Balandin, A.A. and Wang, K.L. (2006) *Handbook of Semiconductor Nanostructures and Nanodevices*, (5-Volume Set), American Scientific Publishers.
- [38] Muller, R.S. and Kamins, T.I. (2002) *Device Electronics for Integrated Circuits*, John Wiley & Sons, Ltd.
- [39] Yu, P.Y. and Cardona, M. (2004) *Fundamentals of Semiconductors: Physics and Materials Properties*, Springer; Fonash, S. (1982) *Solar Cell Device Physics*, Academic Press.
- [40] Gerischer, H. (1979) *Topics in Applied Physics Volume 31: Solar Energy Conversion, Solid-State Physics Aspects* (ed. B.O. Seraphin), Springer-Verlag.

- [41] Bard, A.J. and Faulkner, L.R. (2000) *Electrochemical Methods: Fundamentals and Applications*, John Wiley & Sons, Ltd.
- [42] Bockris, J.O.M., Reddy, A.K.N. and Gamboa-Aldeco, M.E. (2001) *Modern Electrochemistry: Fundamentals of Electrode Processes v. 2a*, Springer.
- [43] Memming, R. (2001) *Semiconductor Electrochemistry*, Wiley-VCH.
- [44] Lipkowsky, J. and Ross, P.N. (1994) *Electrochemistry of Novel Materials*, VCH Publishers.
- [45] Gellings, P.J. and Bouwmeester, H.J.M. (1997) *The CRC Handbook of Solid State Electrochemistry*, CRC Press.
- [46] Nozik, A.J. and Memming, R. (1996) Physical chemistry of semiconductor-liquid interface. *The Journal of Physical Chemistry*, **100**, 13061–13078.
- [47] Gerischer, H. (1970) *Physical Chemistry: An Advanced Treatise*, **9a**, Academic Press.
- [48] Gerischer, H. (1990) The impact of semiconductors on the concept of electrochemistry. *Electrochim Acta*, **35**, 1677–1690.
- [49] Mussini, T. and Longhi, P. (1985) *Standard Potentials in Aqueous Solution* (eds A.J. Bard, R. Parsons and J. Jordan), IUPAC.
- [50] Mavroides, J.G., Kafalas, J.A. and Kolesar, D.F. (1976) Photoelectrolysis of water in cells with SrTiO<sub>3</sub> anodes. *Applied Physics Letters*, **28**, 241–243.
- [51] Ellis, A.B., Kaiser, S.W. and Wrighton, M.S. (1976) Semiconducting potassium tantalate electrodes. *The Journal of Physical Chemistry*, **80**, 1325–1328.
- [52] Green, M.A. (2003) *Third Generation Photovoltaics: Advanced Solar Energy Conversion*, Springer-Verlag.
- [53] Ingler, W.B. Jr. and Khan, S.U.M. (2006) A self-driven p/n-Fe<sub>2</sub>O<sub>3</sub> tandem photoelectrochemical cell for water splitting. *Electrochemical and Solid – State Letters*, **9**, G144–G146.
- [54] Miller, E.L., Rocheleau, R.E. and Deng, X.M. (2003) Design considerations for a hybrid amorphous silicon/photoelectrochemical multijunction cell for hydrogen production. *International Journal of Hydrogen Energy*, **28**, 615–623.
- [55] Miller, E.L., Marsen, B., Paluselli, D. and Rocheleau, R.E. (2005) Optimization of hybrid photoelectrodes for solar water-splitting. *Electrochemical and Solid – State Letters*, **8**, A247–A249.
- [56] Zhu, F., Hu, J., Kunrath, A. et al. (2007) a-SiC:H films used as photoelectrodes in a hybrid, thin-film silicon photoelectrochemical (PEC) cell for progress toward 10% solar-to hydrogen efficiency. *Solar Hydrogen and Nanotechnology – Proceedings of SPIE*, 6650, p. 66500.
- [57] Archer, M.D. (1981) *Photochemical Conversion and Storage of Solar Energy* (ed. J.S. Connolly), Academic Press.
- [58] Hanna, M.C., Lu, Z. and Nozik, A.J. (1997) Hot carrier solar cells. *Proceedings of 1st NREL Conference on Future Photovoltaic Generation. Technology – AIP Conference Proceedings*, 404, pp. 309–316.
- [59] Linkous, C.A., Muradov, N.Z. and Ramser, S.N. (1995) Consideration of reactor design for solar hydrogen production from hydrogen sulfide using semiconductor particulates. *International Journal of Hydrogen Energy*, **20**, 701–709.
- [60] Miller, E.L., Garland, R. and Perret, R. (June (2008)) Photoelectrochemical hydrogen production: DOE PEC working group overview & UNLV-SHGR program subtask. Presented at the DOE Hydrogen Program AMR, Arlington, VA.
- [61] International Energy Agency. (1977) Hydrogen Implementing Agreement. <http://www.ieahia.org/>.
- [62] Grimes, C.A., Varghese, O.K. and Ranjan, S. (2008) *Light, Water, Hydrogen*, Springer.
- [63] Krishnan, R., Licht, S. and McConnell, R. (eds) (2008) *Solar Hydrogen Generation, Toward a Renewable Energy Future*, Springer.
- [64] Murphy, A.B., Barnes, P.R.F., Randeniya, L.K. et al. (2006) Efficiency of solar water splitting using semiconductor electrodes. *International Journal of Hydrogen Energy*, **31**, 1999–2017.
- [65] Heske, C. (2007) Soft X-ray and electron spectroscopy studies of oxide semiconductors for photoelectrochemical hydrogen production. *SPIE proceedings Solar Hydrogen and Nanotechnology II*, San Diego, USA, 26–30 August 2007.
- [66] Huda, M.N., Yanfa, Y., Moon, C.Y. et al. (2008) Density-functional theory study of the effects of atomic impurity on the band edges of monoclinic WO<sub>3</sub>. *Physical Review B*, **77**, 195102.
- [67] Yan, Y. and Wei, S.-H. (2008) Doping asymmetry in wide-bandgap semiconductors: Origins and solutions. *Physica Status Solidi B-Basic Research*, **245**, 641.
- [68] Jaramillo, T.F., Baeck, S.-H., Kleiman-Shwarscstein, A. et al. (2005) Automated electrochemical synthesis and photoelectrochemical characterization of Zn<sub>1-x</sub>Co<sub>x</sub>O thin films for solar hydrogen production. *Journal of Combinatorial Chemistry*, **7**, 264–271.

- [69] Woodhous, M., Herman, G. and Parkinson, B.A. (2005) A combinatorial approach to identification of catalysts for the photoelectrolysis of water. *Chemistry of Materials*, **17**, 4318.
- [70] Yoon, K.H., Seo, D.K., Cho, Y.S. and Kang, D.H. (1998) Effect of Pt layers on the photoelectrochemical properties of a  $\text{WO}_3/p\text{-Si}$  electrode. *Journal of Applied Physics*, **84**, 3954–3959.
- [71] Santato, C., Ulmann, M. and Augustynski, J. (2001) Photoelectrochemical properties of nanostructured tungsten trioxide films. *The Journal of Physical Chemistry B*, **105**, 936–940.
- [72] Solarska, R., Alexander, B.D. and Augustynski, J. (2006) Electrochromic and photoelectrochemical characteristics of nanostructured  $\text{WO}_3$  films prepared by a sol–gel method. *Comptes Rendus Chimie*, **9**, 301–306.
- [73] Weinhardt, L., Blum, M., Bär, M. *et al.* (2008) Electronic surface level positions of  $\text{WO}_3$  thin films for photoelectrochemical hydrogen production. *The Journal of Physical Chemistry C*, **112**, 3078–3082.
- [74] Washizu, E., Yamamoto, A., Abe, Y. *et al.* (2003) Optical and electrochromic properties of RF reactively sputtered  $\text{WO}_3$  films. *Solid State Ionics*, **165**, 175–180.
- [75] Marsen, B., Cole, B. and Miller, E.L. (2007) Influence of sputter oxygen partial pressure on photoelectrochemical performance of tungsten oxide films. *Solar Energy Materials and Solar Cells*, **91**, 1954–1958.
- [76] Alexander, B.D., Kulesza, P.J., Rutkowska, I. *et al.* (2008) Metal oxide photoanodes for solar hydrogen production. *Journal of Materials Chemistry*, **18**, 2298–2303.
- [77] Cole, B., Marsen, B., Miller, E.L. *et al.* (2008) Evaluation of nitrogen doping of tungsten oxide for photoelectrochemical water splitting. *The Journal of Physical Chemistry C*, **112**, 5213–5220.
- [78] Miller, E.L., Paluselli, D., Marsen, B. and Rocheleau, R.E. (2004) Low-temperature reactively sputtered iron oxide for thin film devices. *Thin Solid Films*, **466**, 307–313.
- [79] Duret, A. and Graetzel, M. (2005) Visible light-induced water oxidation on mesoscopic  $\alpha\text{-Fe}_2\text{O}_3$  films made by ultrasonic spray pyrolysis. *The Journal of Physical Chemistry. B*, **109**, 17184–17191.
- [80] Hu, Y.-S., Kleiman-Shwarscstein, A., Forman, A.J. *et al.* (2008) Pt-doped  $\alpha\text{-Fe}_2\text{O}_3$  thin films active for photoelectrochemical water splitting. *Chemistry of Materials*, **20**, 3803–3805.
- [81] Kleiman-Shwarscstein, A., Hu, Y.-S., Forman, A.J. *et al.* (2008) Electrodeposition of  $\alpha\text{-Fe}_2\text{O}_3$  doped with Mo or Cr as photoanodes for photocatalytic water splitting. *The Journal of Physical Chemistry C*, **112**, 15900–15907.
- [82] Kay, A., Cesar, I. and Graetzel, M. (2006) New benchmark for water photooxidation by nanostructured  $\alpha\text{-Fe}_2\text{O}_3$  films. *Journal of the American Chemical Society*, **128**, 15714–15721.
- [83] Zhu, F., Hu, J., Matulionis, I. *et al.* (2009) Amorphous silicon carbide photoelectrode for hydrogen production directly from water using sunlight. *Philosophical Magazine*, **89**, 1478–6443.
- [84] Matulionis, I., Zhu, F., Hu, J. *et al.* (2008) Development of a corrosion-resistant amorphous silicon carbide photoelectrode for solar-to-hydrogen photovoltaic/photoelectrochemical devices. SPIE Solar Energy and Hydrogen 2008, San Diego, USA, 10–14 August 2008.
- [85] Stavrides, A., Kunrath, A., Hu, J. *et al.* (2006) Use of amorphous silicon tandem junction solar cells for hydrogen production in a photoelectrochemical cell. SPIE proceedings Solar Hydrogen and Nanotechnology, San Diego, USA, 13–17 August 2007.
- [86] Yae, S., Kobayashi, T., Abe, M. *et al.* (2007) Solar to chemical conversion using metal nanoparticle modified microcrystalline silicon thin film photoelectrode. *Solar Energy Materials and Solar Cells*, **91**, 224–229.
- [87] Sebastian, P.J., Mathews, N.R., Mathew, X. *et al.* (2001) Photoelectrochemical characterization of SiC. *International Journal of Hydrogen Energy*, **26**, 123–125.
- [88] Bär, M., Bohne, W., Röhrich, J. *et al.* (2004) Determination of the band gap depth profile of the pentenary  $\text{Cu}(\text{In}_{1(x)}\text{Ga}_x)(\text{S}_y\text{Se}_{1(y)})_2$  chalcopyrite from its composition gradient. *Journal of Applied Physics*, **96**, 3857–3860.
- [89] Bär, M., Weinhardt, L., Pookpanratana, S. *et al.* (2008) Depth-resolved band gap in  $\text{Cu}(\text{In,Ga})(\text{S,Se})_2$  thin films. *Applied Physics Letters*, **93**, 244103.
- [90] Bär, M., Weinhardt, L., Heske, C. *et al.* (2008) Chemical structures of the  $\text{Cu}(\text{In,Ga})\text{Se}_2/\text{Mo}$  and  $\text{Cu}(\text{In,Ga})(\text{S,Se})_2/\text{Mo}$  interfaces. *Physical Review B-Condensed Matter*, **78**, 075404.
- [91] Marsen, B., Cole, B. and Miller, E.L. (2008) Photoelectrolysis of water using thin copper gallium diselenide electrodes. *Solar Energy Materials & Solar Cells*, **92**, 1054–1058.
- [92] Jaramillo, T.F., Jørgensen, K.P., Bonde, J. *et al.* (2007) Identification of active edge sites for electrochemical  $\text{H}_2$  evolution from  $\text{MoS}_2$  nanocatalysts. *Science*, **317**, 100–102.
- [93] Deutsch, T.G., Koval, C.A. and Turner, J.A. (2006) III–V nitride epilayers for photoelectrochemical water splitting: GaPN and GaAsPN. *The Journal of Physical Chemistry B*, **110**, 25297–25307.
- [94] Khaselev, O. and Turner, J.A. (1998) A monolithic photovoltaic photoelectrochemical device for hydrogen production via water splitting. *Science*, **280**, 425–427.

